Magnetic hybrid Pd/Fe-oxide nanoparticles meet the demands for ablative thermo-brachytherapy

Rogier van Oossanen, Alexandra Maier, Jérémy Godart, Jean-Philippe Pignol, Antonia G. Denkova, Gerard C. van Rhoon & Kristina Djanashvili

View supplementary material

Published online: 08 Jan 2024.

Submit your article to this journal

Article views: 173

View related articles

View Crossmark data

Taylor & Francis
Taylor & Francis Group

🔓 OPEN ACCESS | Check for updates

Magnetic hybrid Pd/Fe-oxide nanoparticles meet the demands for ablative thermo-brachytherapy

Rogier van Oossanen[a,b], Alexandra Maier[c], Jérémy Godart[a], Jean-Philippe Pignol[a], Antonia G. Denkova[b], Gerard C. van Rhoon[a] and Kristina Djanashvili[c]

[a]Department of Radiotherapy, Erasmus MC Cancer Institute, University Medical Center, Rotterdam, The Netherlands; [b]Department of Radiation Science and Technology, Delft University of Technology, Delft, The Netherlands; [c]Department of Biotechnology, Delft University of Technology, Delft, The Netherlands

ABSTRACT

Objective: To investigate the potential of hybrid Pd/Fe-oxide magnetic nanoparticles designed for thermo-brachytherapy of breast cancer, considering their specific loss power (*SLP*) and clinical constraints in the applied magnetic field.

Methods: Hybrid nanoparticles consisting of palladium-core and iron oxide shell of increasing thickness, were suspended in water and their *SLP*s were measured at varying magnetic fields (12–26 mT peak) and frequencies (50–730 kHz) with a commercial alternating magnetic field generator (magneTherm™ Digital, nanoTherics Ltd.).

Results: Validation of the heating device used in this study with commercial HyperMag-C nanoparticles showed a small deviation (±4%) over a period of 1 year, confirming the reliability of the method. The integration of dual thermometers, one in the center and one at the bottom of the sample vial, allowed monitoring of homogeneity of the sample suspensions. *SLP*s measurements on a series of nanoparticles of increasing sizes showed the highest heating for the diameter of 21 nm (*SLP* = 225 W/g) at the applied frequencies of 346 and 730 kHz. No heating was observed for the nanoparticles with the size <14 nm, confirming the importance of the size-parameter. The heating ability of the best performing Pd/Fe-oxide-21 was calculated to be sufficient to ablate tumors with a radius ±4 and 12 mm using 10 and 1 mg/mL nanoparticle concentration, respectively.

Conclusions: Nanoparticles consisting of non-magnetic palladium-core and magnetic iron oxide shell are suitable for magnetic hyperthermia/thermal ablation under clinically safe conditions of 346 kHz and 19.1 mT, with minimal eddy current effects in combination with maximum *SLP*.

1. Introduction

Heat has been successfully applied in cancer treatment either using hyperthermia [1] to enhance the effectiveness of chemo- and radiotherapy [2] or to thermally ablate tissues [3]. During the last decades, magnetic nanoparticle hyperthermia (MNH) has gained attention as a potential modality for delivering thermal treatment [4–8]. One advantage of MNH is that the magnetic nanoparticles (MNPs) can be delivered to the tumor site percutaneously using fine needles. Then the MNPs are exposed to an alternating magnetic field (AMF). Depending on their magnetic properties, the MNPs interact strongly with the magnetic field and subsequently heat is produced [9, 10]. By injecting the MNPs selectively into the tumor, a highly localized thermal dose is delivered, which enables efficient hyperthermia and precise heat treatment. From a clinical perspective, MNP thermal ablation corresponds to a minimal invasive procedure [11].

The feasibility of MNH depends on the nanoparticles being able to provide sufficient heating power, which is expressed as the specific loss power (*SLP*), derived from the total heating power dissipated from the MNPs to the environment (*P*) divided by the mass of iron in the MNPs (m_{Fe}) [12] (Eq. (1)), and expressed in W/g [9, 10, 12].

$$SLP = \frac{P}{m_{Fe}} \tag{1}$$

Since there is still no standard method or equipment to measure *SLP*, the comparison of MNPs batches based on their *SLP* values should be done with conscious consideration of the conditions necessary for a reliable assessment. The literature shows that *SLP* measurements are highly dependent on the heating device used, as well as on the analysis method and the applied field conditions. A study by Wells et al. has demonstrated that the *SLP* measured on the same batch of MNPs varies on average 30 to 40% between different

---

laboratories [13]. At the same time, the deviations in the outcome of the measurements performed at the same laboratory were less than 5% in most laboratories. This study indicates that although results cannot be directly compared between laboratories, results from the same laboratory on different MNP batches can be accurately compared. This, therefore, allows to compare different, internally produced MNPs for *SLP* performance, as long as all batches are measured using the same methodology and experimental set-up.

Currently, there is growing interest for the use of thermal ablation as alternative for surgery of early breast cancer [14–16]. In this indication, MNPs thermal ablation has the potential to become a minimally invasive treatment under light sedation, which is more economical and may lead to an improved cosmetic result as no breast tissue is removed [14, 17–20]. Recently, we have reported on novel hybrid MNPs composed of a non-magnetic palladium core and a magnetic iron oxide shell for combined thermal ablation and low dose-rate (LDR) brachytherapy using[103]Pd [21, 22]. In this concept, MNPs are intended to be incorporated into gel-like seeds, which can be implanted into a tumor with high precision using conventional brachytherapy equipment. The subsequent exposure to AMF leads to thermal ablation of the tumor bulk, while the radioactive MNPs decay slowly, delivering a therapeutic dose over weeks without requiring multiple hospital visits as it is done with external beam radiotherapy [23]. As the ablation and adjuvant radiotherapy are realized in a single one-stop-shop procedure, this could significantly reduce patient burden and treatment time.

For this novel treatment to be successful, the first requirement is that the hybrid MNPs can induce high *SLP*, which also means that a lesser amount of material is needed for intra-tumoral injection. Furthermore, there are also limits to the maximum magnetic field strength and frequency of an AMF that can be safely applied to patients. The AMF limit is reported to be around $5 \cdot 10^9$ $Am^{-1}s^{-1}$ for hyperthermia applications using coils with a diameter of around 10 cm [24, 25]. This AMF limit is expressed as the product of magnetic field strength (*H*-field) in Am^{-1} and the frequency (s^{-1}). However, our setup is calibrated using the magnetic flux density field (*B*-field), which is closely related to the *H*-field as follows from Eq. (2). Therefore, the AMF limit can be rewritten as approximately 6.3×10^3 Ts^{-1}, assuming $\mu_r \approx 1$ for air. If this limit is exceeded, eddy currents might be induced in healthy tissue, causing unwanted and nonselective heating and ultimately burns. Therefore, the heating performance of MNPs should not only be evaluated using *SLP* values, but the clinical limitations on magnetic field strength and frequency should also be considered to enable clinical MNH.

$$B = \mu_0 \mu_r H \tag{2}$$

In this study we investigated several core–shell palladium iron oxide MNPs (Pd/Fe-oxide-n) with the sizes (n) ranging from 10 to 21 nm, prepared earlier in our laboratory [21]. The *SLP* of these MNPs was determined for frequencies ranging from 50 kHz to 730 kHz and compared to find the optimal batch for clinical application, keeping the AMF limit in mind. To ensure consistency of *SLP* measurements, commercial MNPs were used first to validate the reliability of the heating device.

2. Materials and methods

2.1. Nanoparticles heating device

Adiabatic heating experiments to assess *SLP* were performed with the magneTherm[TM] Digital (nanoTherics Ltd. (Warrington, UK)) and a 50 mm diameter coil device. The device is a fully automated and integrated MNPs heating device, combining a multi-frequency AMF power supply unit with a set of coils of various sizes. The device is connected to a water cooler/heater, enabling to control the coil temperature. This setup can generate high-intensity AMF with frequencies ranging from 50 to 730 kHz and maximum magnetic field strengths from 12 to 26 mT peak, depending on the frequency. The system includes two glass fiber thermometers (Osensa[1] PRB-G40 2.0 M-STM-MRI sensor) with a 1 mm outer diameter, compatible with strong magnetic fields for undisturbed temperature measurements. The magnetic field strengths delivered to the MNPs were measured using a 2D HF Magnetic Field Probe (AMF Life Systems LCC[2]) in combination with a TBS 1202B-EDU Digital Oscilloscope (Tektronix Inc.[3]). An overview of the available frequencies and the corresponding measured maximum magnetic field strengths is given in Table 1.

The device used for the *SLP* measurements was cooled with water circulating through the coil at 20 °C, and heat loss was prevented by placing the plastic sample vial in an insulated polystyrene holder. The temperature was assessed by the fiber-optic thermometers inserted through the holes in the lid of the sample vial, with one thermometer positioned in the center and the other at the bottom of the sample vial (Figure 1). This setting allows for monitoring of the heating power distribution within the whole sample volume and ensures the suspension stability, as sedimentation of the MNPs would lead to a higher temperature at the bottom of the sample.

2.2. Magnetic nanoparticles and sample preparation

The Pd/Fe-oxide-n MNPs were synthesized in-house and characterized, which has been published previously by Maier et al. [21]. The commercial iron oxide nanoparticles, HyperMAG-C, coated with dimercaptosuccinic acid (DMSA), were purchased

Table 1. Overview of the AMF frequencies generated by the magneTherm[TM] Digital and the corresponding measured maximum magnetic field peak strengths including standard deviation ($n = 3$).

Frequency (kHz)	50	159	188	251	297	346	390	454	570	730
Magnetic field (mT)	26.36 ± 0.12	21.06 ± 0.04	18.66 ± 0.03	21.80 ± 0.04	20.74 ± 0.09	19.13 ± 0.12	16.81 ± 0.02	16.18 ± 0.12	13.20 ± 0.03	12.33 ± 0.04
Field-Frequency product (T s^{-1})	1318	3349	3508	5472	6160	6619	6556	7346	7524	9013

from nanoTherics Ltd (Warrington, UK). These MNPs are available in an aqueous suspension with a stock concentration of 10 mg(Fe)/mL. All Pd/Fe-oxide MPNs used in this study (Table 2) were coated with DSPE-PEG$_{2000}$-COOH (DSPE = 1,2-distearoyl-sn-glycero-3-phosphoethanolamine, PEG = carboxy polyethylene glycol) following the procedure described in Ref. [21] and dispersed in water prior to the measurements. The batch Pd/Fe-oxide-21 was used as a model to study the effect of the surfactants: DSPE-PEG$_{2000}$-COOH, DSPE-PEG$_{2000}$-NH$_2$, DSPE-PEG$_{5000}$-NH$_2$, DSPE-PEG$_{2000}$-OCH$_3$ and Si-PEG$_{5000}$-COOH [21]. All surfactants were purchased from Avanti Polar Lipids (Alabaster, USA).

Magnetic properties were assessed by a superconducting quantum interference device (SQUID) using a MPMS LX magnetometer from Quantum Design (San Diego, USA). About 1 mg of dry MNPs was used and the hysteresis loops were obtained under continuously increasing static magnetic field at 300 K. The samples were prepared by suspending approximately 4 mg$_{Fe}$ of dry MNPs in 1 mL of Milli-Q water and intense stirring to homogenize the sample, although the homogeneity of the opaque suspensions could not be verified

by eye. Directly after mixing, 1 mL of each suspension was transferred to a 2 ml plastic vial covered with a screw cap with two 1 mm holes to guide the fiber-optic thermometers. After heat measurements, the exact iron concentration of the sample was determined by inductively coupled plasma optical emission spectrometer ICP-OES Optima 8000 from Perkin Elmer (Groningen, The Netherlands) for the *SLP* calculations.

2.3. Specific loss power measurements

For all *SLP* measurements the temperature was tracked before the exposure until the sample temperature variation was less than 0.05 °C/min, indicating the sample has reached an equilibrium with the environment. Then, the sample was exposed to the magnetic field for 60 s while constantly measuring the temperature. The sample was allowed to cool naturally to its equilibrium temperature before starting the next measurement. The *SLP* were calculated using the ΔT between 5 and 50 s, to discard non-linear effects of the device caused during the starting and stopping of magnetic field [26].

2.4. Intra-laboratory reliability of SLP measurements

The focus of this study is to investigate the *SLP* of the hybrid Pd/Fe-oxide MNPs developed in our laboratory and the relations of the corresponding *SLP* to magnetic field strength and frequency. As explained earlier, the *SLP* values commonly reported to express the heat generation capacity of MNPs are influenced by the procedure and the device used [13]. To ensure intra-laboratory reliability of the experimental setup, we performed a series of *SLP* measurements using commercial HyperMag-C nanoparticles. A vial containing an aqueous MNPs suspension (10 mg$_{Fe}$/mL) was placed in the coil and the induced heating was measured at a frequency of 346 kHz with a field strength of 19.2 mT. This calibration measurement was repeated under the same conditions for 12 months to assess the long-term performance of the magneTherm^{TM} Digital device. With a total of 21 measurements, ranging between 115 W/g and 132 W/g, the standard deviation was determined to be 4.9 W/g (3.9%) (Type A evaluation of standard uncertainty) as listed in Table S1. This standard deviation has been used as measurement uncertainty (Type B evaluation of standard uncertainty) for all other samples. In addition, a fresh HyperMag-C suspension was measured midway (after 6 months), which provided a comparable *SLP* value indicative of the maintained colloidal
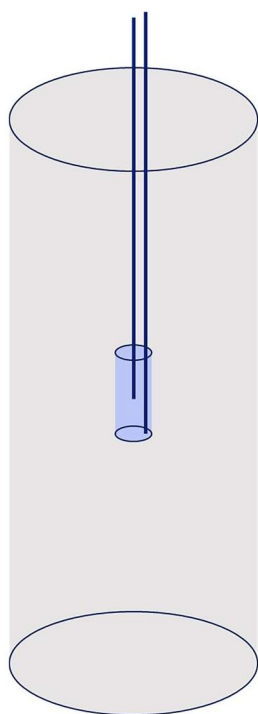

Figure 1. Schematic drawing of the insulated polystyrene sample holder (grey) containing the plastic sample vial (blue) and two glass fiber thermometers.

Table 2. Overview of MNPs evaluated in this study and their corresponding magnetic properties [21].

MNPs	Diameter (nm)	M_s (300 K/5 K) (emu/g$_{NP}$)	H_c (300 K/5 K) (Oe)	T_B (K)	Batch name in Ref. [21]
Fe-oxide-comm	15	—[a]	—[a]	—[a]	—[b]
Pd/Fe-oxide-10	10	20.5/26.4	10/466	30	Exp_[surf]/[Fe] = 2
Pd/Fe-oxide-12	12	28.1/36.9	19/236	23	Exp_DPE
Pd/Fe-oxide-13	13	45.1/52.1	8/287	40	Exp_3 °C
Pd/Fe-oxide-16	16	39.9/46.5	9/56	120	Exp_ODE:DPE(1:1)
Pd/Fe-oxide-18	18	55.4/63.6	4/13	160	Exp_DBE
Pd/Fe-oxide-19	19	57.5/63.7	6/213	130	Exp_7 °C
Pd/Fe-oxide-20	20	58.7/67.9	8/20	180	Exp_standard
Pd/Fe-oxide-21	21	61.4/69.2	12/67	200	Exp_10mg

[a]not determined; [b]commercial MNPs.

stability of the sample used for the long-term measurements. It is noteworthy that a slight decrease in the suspension stability became visible only after 10 months and became obvious after 12 months. The *SLP* of the 12-month-old sample was measured 5 times in a row, with the first measurement being 119 W/g, each consecutive measurement slightly less and the last measurement being only 101 W/g, as it can be seen in Figure S1. This underlines the importance of a sample that is stable in suspension and the need to properly vortex the sample before each measurement.

2.5. SLP calculations

The *SLP* values, typically calculated using Eq. (3), account for two heat loss mechanisms. When the system is adiabatic, meaning the heat loss to the environment is negligible compared to the sample heating, *P* is calculated as follows:

$$P = C \cdot m_m \cdot \frac{dT}{dt} \tag{3}$$

where *C* is the specific heat capacity of the medium (water), m_m is the mass of the medium, *T* is the temperature and *t* is the time [27].

In a non-adiabatic system, the energy loss to the environment must be compensated using the Corrected Slope Method (CSM) [27]:

$$P - L\Delta T = C \cdot \frac{dT}{dt} \tag{4}$$

where *L* is the linear loss factor that describes the heat loss to the environment as a function of ΔT (the temperature difference between the sample T_s and the environment T_0) and *L* is a sample-specific constant that is derived from the cooling curve after the magnetic field has been turned off. The CSM is only valid for the values of ΔT where the heat loss to the environment is linearly proportional to ΔT.

Figure 2 suggests that it takes at least 30 min for a sample in an insulated holder to cool down to ambient temperature ($\Delta T < 20\,°C$) after stopping the AMF. The cooling rate

(0.75 °C/min) is around 4% of the heating rate (17.9 °C/min), which is close to the error in the *SLP* measurements as reported in Section 2.4. When comparing the adiabatic methods and CSM for calculating the *SLP*, the difference in the two methods was smaller than the measurement uncertainty. Therefore, the system was assumed to be adiabatic for $\Delta T < 20\,°C$.

2.6. Sample inhomogeneity

Although all samples were thoroughly mixed prior to measurements, the heat generated by some, not included, MNPs batches was not homogeneous. Figure 3 represents temperature curves of an old, oxidized HyperMag-C sample, which has become unstable in suspension. Figure 3(A) shows a linear increase in sample core and bottom temperatures measured immediately after intense vortexing, with a slightly slower cooling rate measured at the bottom. In contrast, when the measurements were done without vortexing the same sample, different heating/cooling rates were measured at the two locations, indicating aggregation and sedimentation of the MNPs (Figure 3(B)). The sedimentation of the MNPs was not visible to the naked eye and was only observed by comparing the two temperature profiles. This underlines the importance of two temperature probes to check the stability of the suspensions for proper investigations of *SLP*s.

3. Results and discussion

3.1. MNP size effect

The hybrid Pd/Fe-oxide MNPs batches *SLP*, with characteristics detailed in Table 2, were measured at the frequencies of 50, 346 and 730 kHz (Figure 4) using the concentrations determined by ICP-OES (Table S2). The first observation shows that the *SLP* values measured at 50 kHz remain low (40 W/g) for all MNPs sizes and MNPs below 13 nm do not heat at all regardless of the frequencies. Above this size, the
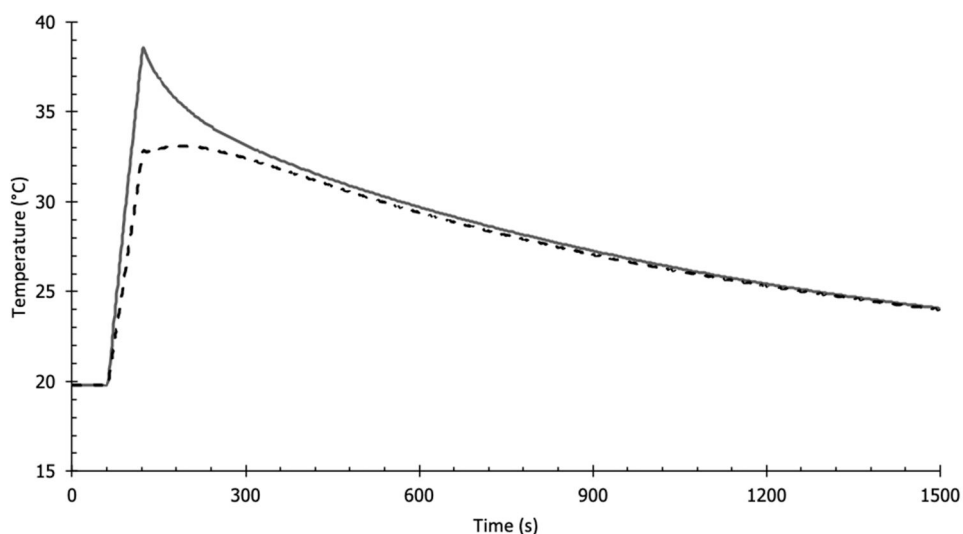

Figure 2. Heating/cooling curve of HyperMag-C sample in the insulated sample holder. The solid and the dashed lines represent the core and the bottom temperatures of the sample, respectively.
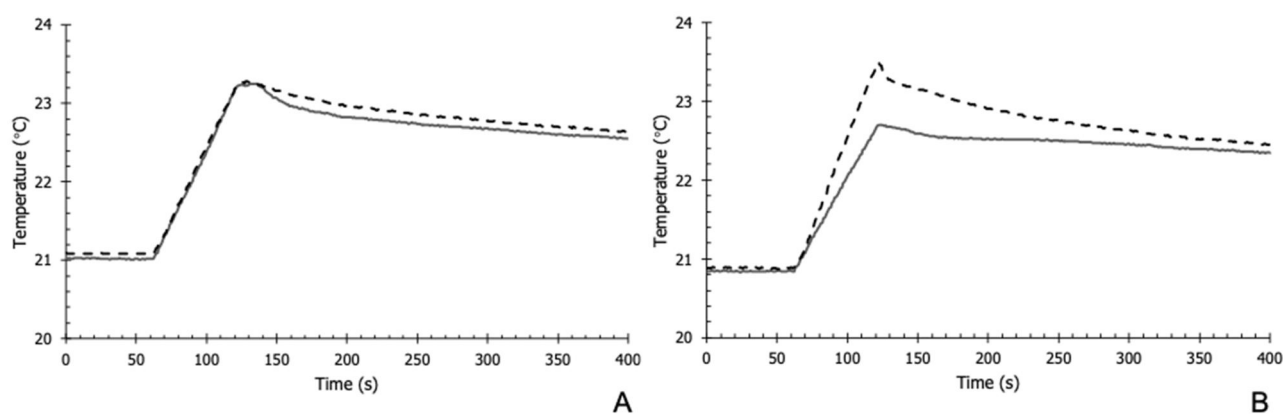
Figure 3. Heating curves of an old, unstable batch of HyperMag-C MNPs obtained with two thermometers placed at the center (solid line) and the bottom (dashed line) of the sample measured immediately after (A) or a few hours after (B) rigorous stirring.
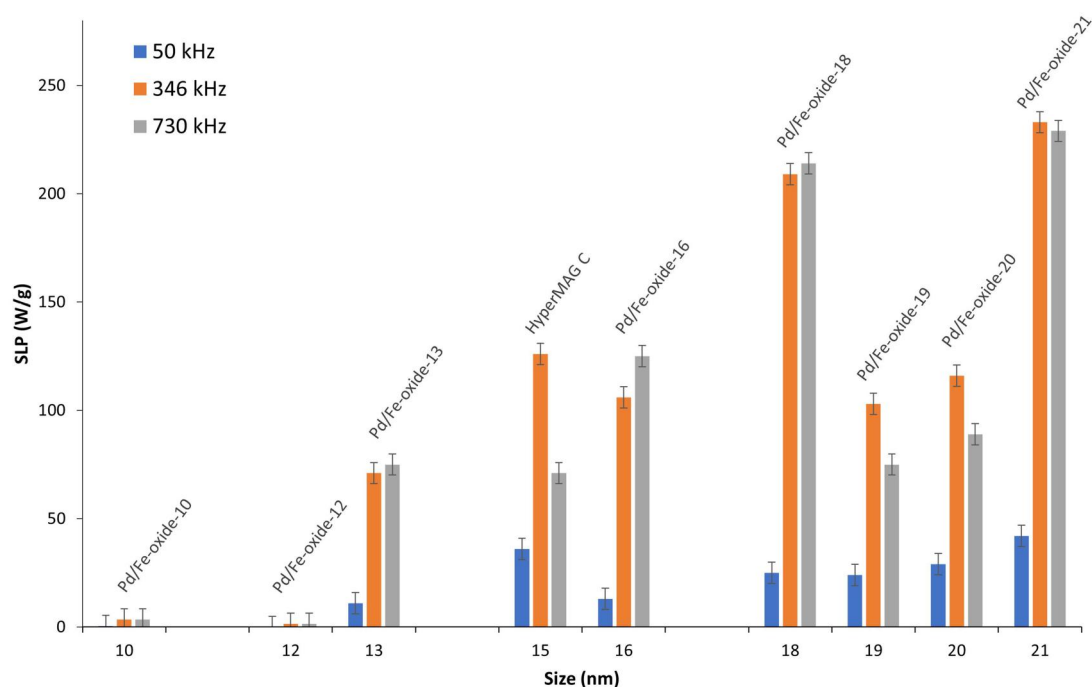

Figure 4. The *SLP* of all synthesized Pd/Fe-oxide-n MNPs vs their size (n) measured at 50, 346 and 730 kHz. Commercial nanoparticles (Fe-oxide-comm, HyperMag-C) with the size of 15 nm are also included for comparison.

SLP of all MNPs typically show an increasing heating trend with size, however, some interesting observations can be made. For instance, the *SLP* of Pd/Fe-oxide-n ($n = 13$, 18, 21) are similar at 346 and 730 kHz, while Pd/Fe-oxide-16 shows more heating at 730 kHz. Interestingly, the opposite is true for Pd/Fe-oxide-19 and Pd/Fe-oxide-20, where more heating is detected at 346 kHz. The trend of increasing *SLP* with increasing sizes, at least in the range 12 to 20 nm, has also been previously reported for conventional iron oxide MNPs [28–30]. The *SLP* of the three largest samples, Pd/Fe-oxide-n ($n = 19$, 20, 21) was determined for all frequencies available on the magneTherm™ Digital (Table S3). These measurements confirmed that the largest *SLP* values are observed at 346 kHz, while at higher frequencies the *SLP* either plateaus ($n = 21$) or gradually decreases slightly ($n = 19$, 20).

In an attempt to understand the difference in frequency dependence, we took a closer look at the other parameters of these MNPs, as previously reported by Maier et al. [21] and now shown in Table 2. There is a possibility that Pd/Fe-oxide-19 and Pd/Fe-oxide-20 MNPs have lower saturation magnetization, which limits their *SLP*. However, when comparing the saturation magnetization of the samples, Pd/Fe-oxide-19 and Pd/Fe-oxide-20 do not appear to be substantially different from the other samples. When looking at the blocking temperature T_B, a measure of the anisotropy of the MNPs [31], there is also no clear difference between Pd/Fe-oxide-19, Pd/Fe-oxide-20 and the other samples. The size and size distribution of the samples, whose TEM images are given in Figure S1, do not provide any indication either. Although the size distribution of Pd/Fe-oxide-20 can be described as narrow compared to most other samples, Pd/Fe-oxide-19 MNPs exhibit a broader size distribution comparable to that of Pd/Fe-oxide-21 and Pd/Fe-oxide-16 MNPs [21].

In general, *SLP* is higher at 730 kHz compared to 346 kHz. However, for some samples, among which Pd/Fe-oxide-19 and Pd/Fe-oxide-20, this is not the case. The decrease in *SLP*

at 730 kHz could indicate that the frequency is approaching the so-called blocking frequency, which is too high for the magnetization of the MNPs to revert before the direction of the external field is changed again [9]. Further investigation on *SLP* of these samples at frequencies beyond 730 kHz could give more insight into the effects of the blocking frequency.

Another parameter, related to the saturation magnetization, is the so-called anisotropy field H_k. This is the external field intensity required to completely change the magnetization orientation, e.g. the external field at which the sample reaches its saturation magnetization. In Figure 5 it can be seen that within the field strengths used (±300 Oe max) the magnetization of the sample is not saturated yet, indicating

that the H_k field is not reached. This implies that the MNPs are still in the regime, where an increase in magnetic field strength would increase magnetization, and thus increase *SLP*. Therefore, it can be concluded that H_k is not a limiting factor in the *SLP* of the samples in this study.

3.2. Blocking temperature effect

In Figure 6, the *SLP* values of the samples are plotted against the corresponding blocking temperatures (T_B) as determined using Zero Field Cooling (ZFC). The blocking temperature generally increases with increasing MNP size [21]. For both size and T_B, a trend of increasing *SLP* is observed. Samples Pd/Fe-oxide-10 and Pd/Fe-oxide-12, which did not show
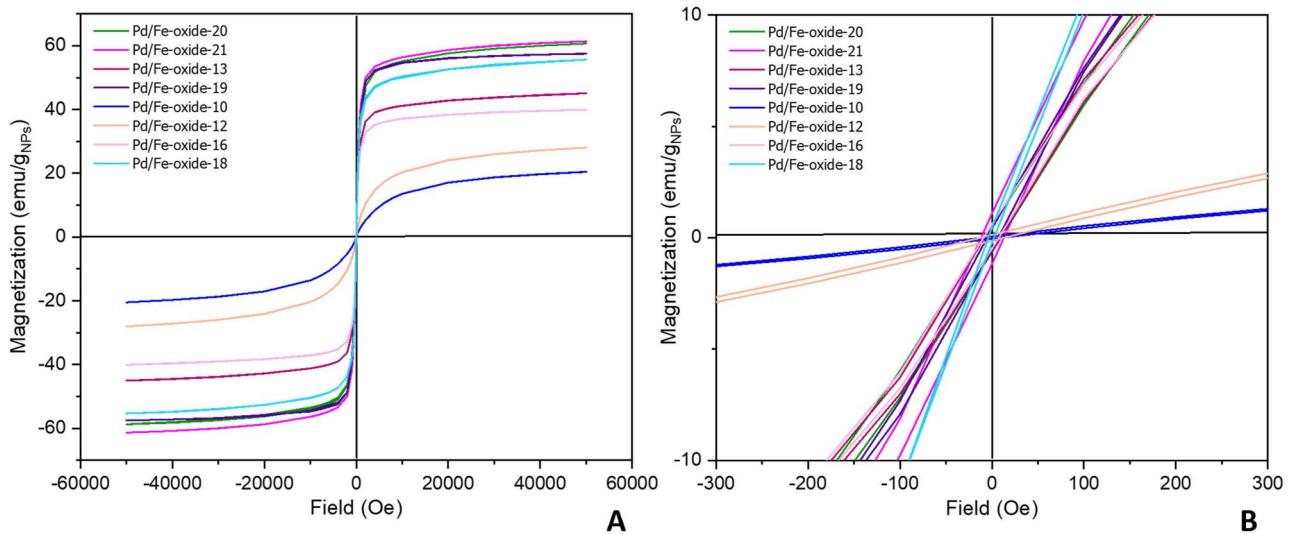

Figure 5. Magnetization curves measured with dry Pd/Fe-oxide MNPs at 300 K (A) as described in [21] and magnification of the x-axis showing coercivities H_c at static field.
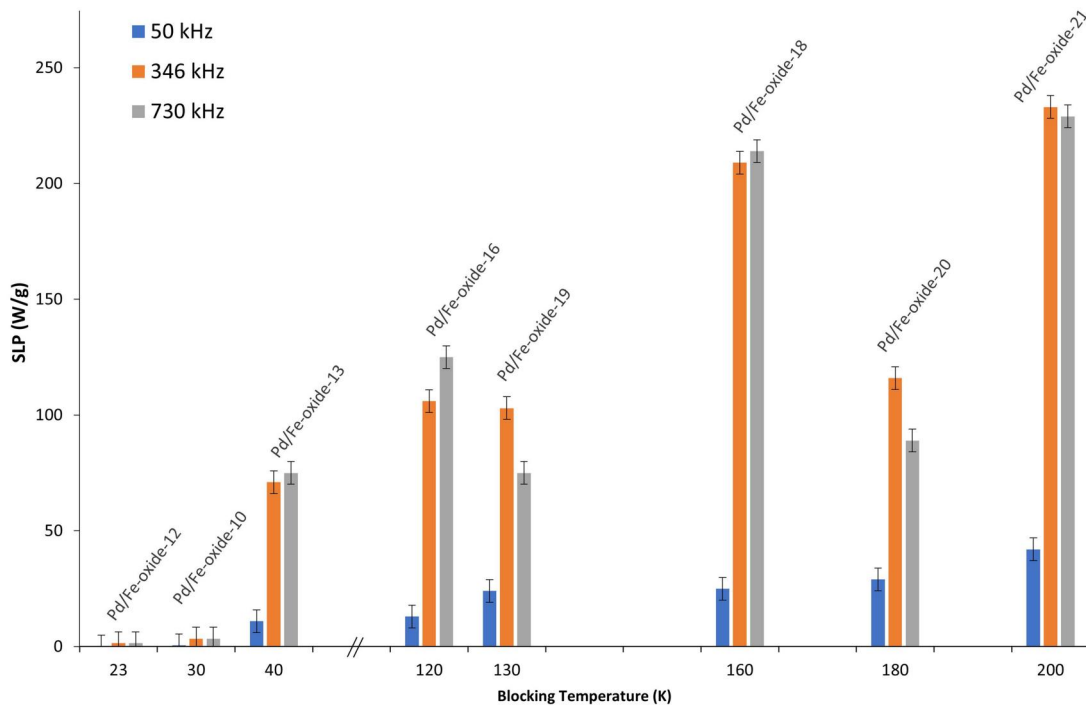

Figure 6. Blocking temperatures of the Pd/Fe-oxide-n MNPs [21] vs their *SLP* at 50, 346 and 730 kHz.

significantly high *SLP*, also have the lowest T_B. Interestingly, the T_B of Pd/Fe-oxide-13 is only slightly higher, while the *SLP* is much higher. This suggests the size is more of a limiting factor than T_B for these MNPs.

3.3. Surfactant effect

Common practice to increase the colloidal stability of the suspension of MNPs is to coat their surface with surfactant molecules, of which numerous options are available [32]. Therefore, in this study we also investigated the impact of four different surfactants on the *SLP* performance. To do this, Pd/Fe-oxide-21 MNPs were coated with various polyethylene glycol (PEG) derivatives and *SLP* were measured at 346 kHz and 19.2 mT. The first sample was coated with DSPE-PEG$_{2000}$-COOH, which is also used for all the samples mentioned in the previous sections. The other three samples were coated with DSPE-PEG$_{2000}$-methoxy, DSPE-PEG$_{2000}$-NH$_2$ and DSPE-PEG$_{5000}$-NH$_2$ respectively. In this experiment no significant difference in *SLP* was measured between these four samples, with the *SLP* ranging from 188 to 205 W/g.

3.4. SLP clinical application

We have investigated various MNPs and determined their *SLP* in order to find the best performing one for clinical applications. There have been many studies evaluating the heat dissipation from MNPs for hyperthermia and the corresponding MNPs distribution [33–37], which can become rather complex. For our purpose, we used a simple first approximation introduced by Dutz and Hergt [24], who proposed a formula to determine the minimal *SLP* to elevate the temperature in a spherical tumor by ΔT, assuming a homogeneous MNPs concentration c and a tumor radius R:

$$SLP = \frac{\Delta T \cdot 3\lambda}{c \cdot R^2} \tag{5}$$

Here λ is the heat conductivity of tissue, assumed to be 0.64 WK^{-1}m^{-1} [38]. This equation indicates that the smaller the tumor, the higher the *SLP* needed to reach the same temperature increase.

Using Eq. (5) and assuming an average concentration of 10 mg/mL of MNPs is achievable by implantation of the MNPs, a 2D color-plot with *SLP*, *R* and ΔT was made (Figure 7). Thermal ablation treatment requires a temperature increase of at least 15 °C or higher above the body temperature [39]. Clearly, MPNs Pd/Fe-oxide-21(line a) and Pd/Fe-oxide-18 (line b), with *SLP* greater than 200 W/g at both 346 kHz and 730 kHz, have the potential to thermally ablate tumors with a radius as small as 4 mm when using an average concentration of 10 mg/mL of MNPs. In the case of Pd/Fe-oxide-20 (line c) it can be seen that an *SLP* < 120 W/g can still lead to ablation of the tumor larger than 5 nm. An overview of the samples with their corresponding *SLP* (> 50 W/g) and the minimum tumor size that can be thermally ablated is given in Table 3.

Table 1 shows that at 346 kHz, the *Hf* value (6619 Ts^{-1}) is close to the AMF limit (6300 Ts^{-1}) for clinical application, while at 730 kHz the *Hf* value (9013 Ts^{-1}) is 35% higher. This means that to use thermal ablation safely at 730 kHz, the magnetic field strength must be lowered by 35% to remain below the AMF limit. However, this would significantly reduce the *SLP* and is therefore undesirable. At 50 kHz, the *SLP* is only about 40 W/g, but the *Hf* value around 1300 Ts^{-1} is almost 5 times lower than the AMF limit. A magnetic field strength 5 times higher, at 150 mT, would be needed, but we could not determine *SLP* at these high magnetic field strengths due to hardware limitations. As the heating power increases linearly with frequency and exponentially with field strength, a 150 mT field at 50 kHz would theoretically provide more heating than 19 mT and 346 kHz, while the *Hf* value remains the same. However, we foresee that it might be challenging to design a clinical system capable of generating such a strong field, because the required current would be so large that this would in turn introduce new demands for coil cooling, safety and other technological aspects. At the same time, it has been reported that at very high field strengths, the increase in *SLP* is limited as it becomes stable and does not raise further [40]. Taking all these factors into account, our results suggest that the best-case scenario that
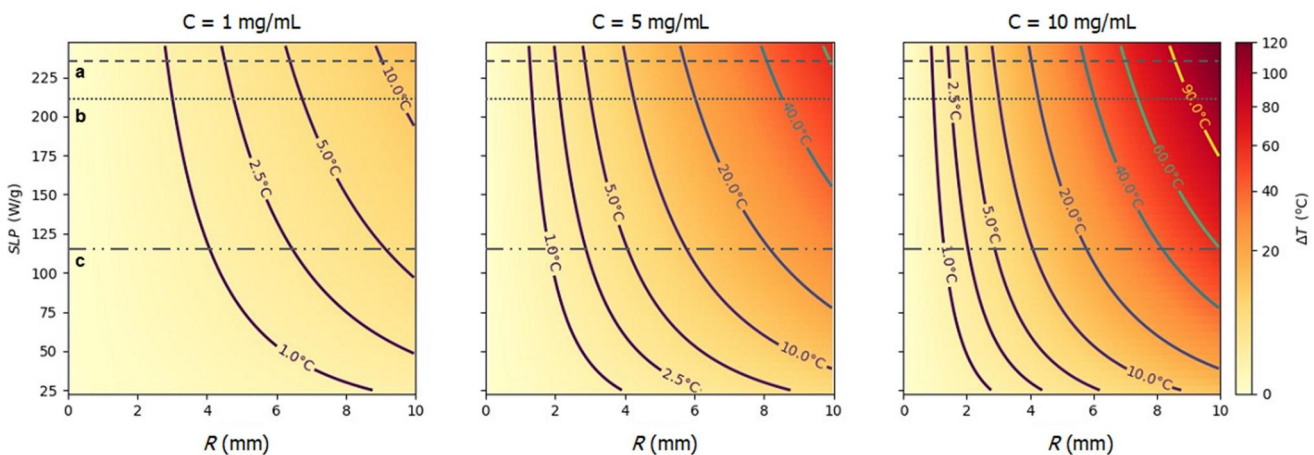

Figure 7. Modeled relationship between *SLP* and tumor radius, and the achievable temperature increase within the tumor with homogeneously distributed MNPs. The lines represent the actual *SLP* values of Pd/Fe-oxide-21 (A), Pd/Fe-oxide-18 (B) and Pd/Fe-oxide-20 (C) measured at the optimal field (19 mT) and frequency (345 kHz) combination.

Table 3. The Pd/Fe-oxide-n MNP batches and corresponding *SLP* measured at 346 kHz. For each sample the minimum tumor radius R_{min} that can be thermally ablated ($\Delta T = 15\,°C$) is calculated using Eq. (5), any tumor with a radius larger than R_{min} can be thermally ablated. The shaded samples have the highest *SLP* and are therefore most suitable for thermal ablation.

Sample	*SLP* (W/g)	R_{min} (mm) $c = 1$ mg/mL	R_{min} (mm) $c = 5$ mg/mL	R_{min} (mm) $c = 10$ mg/mL
Pd/Fe-oxide-21	233	11.1	5.0	3.5
Pd/Fe-oxide-18	209	11.7	5.2	3.7
Pd/Fe-oxide-20	116	15.8	7.1	5.0
Pd/Fe-oxide-16	106	16.5	7.4	5.2
Pd/Fe-oxide-19	103	16.7	7.5	5.3
Pd/Fe-oxide-13	71	20.1	9.0	6.4

can be safely realized includes Pd/Fe-oxide-21 MNPs heated at 346 kHz. It would be interesting to investigate frequencies between 50 kHz and 346 kHz at higher magnetic field strengths, where higher heating might be obtained for the same *Hf* value.

4. Conclusion

Comparing the different hybrid Pd/Fe-oxide MNPs and their corresponding heating performance, our results suggest a strong heating power dependency on MNPs size and blocking temperature, comparable to commercial iron oxide MNPs. A trend of greater *SLP* with increasing size was observed, along with an absence of heating power at small MNPs sizes. Therefore, the finding that the best performing MNPs are Pd/Fe-oxide-21 with the largest diameter of 21 nm at both 346 kHz and 730 kHz, is in line with the reported observations for iron oxide MNPs.

We conclude that within the frame of our experimental design, Pd/Fe-oxide-21 MNPs at a concentration of 5 mg/mL can effectively ablate tumors of 5 mm or larger. Accounting for the AMF limit for safe clinical application, we recommend using radioactive Pd/Fe-oxide hybrid MNPs for thermal ablation with a 346 kHz field to minimize eddy current effects while maximizing *SLP*.

Notes

1. OSENSA Innovations Corp, 8672 Commerce Ct., Burnaby, BC, Canada V5A 4N7, https://www.osensa.com/.
2. AMF Life Systems LCC, 1388 Atlantic Boulevard, Auburn Hills, MI 48326 USA, https://amflife.com/.
3. Tektronix UK Ltd. The Capitol Building, Oldbury, Bracknell, Berkshire, RG12 8FZ, UK, https://www.tek.com/.

Disclosure statement

No potential conflict of interest was reported by the author(s).

Funding

Data availability statement

The data underlying this work is available upon request from the corresponding author.

References

[1] Gas P. Essential facts on the history of hyperthermia and their connections with electromedicine. Przegl Elektrotech. 2011;87:37–40.

[2] Falk MH, Issels RD. Hyperthermia in oncology. Int J Hyperthermia. 2001;17(1):1–18. doi: 10.1080/02656730150201552.

[3] Stauffer PR, Goldberg SN. Introduction: thermal ablation therapy. Int J Hyperthermia. 2004;20(7):671–677. doi: 10.1080/02656730400007220.

[4] Kozissnik B, Bohorquez AC, Dobson J, et al. Magnetic fluid hyperthermia: advances, challenges, and opportunity. Int J Hyperthermia. 2013;29(8):706–714. doi: 10.3109/02656736.2013.837200.

[5] Giustini AJ, Petryk AA, Cassim SM, et al. Magnetic nanoparticle hyperthermia in cancer treatment. Nano Life. 2010;1(02):17–32. doi: 10.1142/S1793984410000067.

[6] Ashikbayeva Z, Tosi D, Balmassov D, et al. Application of nanoparticles and nanomaterials in thermal ablation therapy of cancer. Nanomaterials (Basel). 2019;9(9):1195. doi: 10.3390/nano9091195.

[7] Jordan A. Hyperthermia classic commentary: 'Inductive heating of ferrimagnetic particles and magnetic fluids: physical evaluation of their potential for hyperthermia' by andreas Jordan et al., international journal of hyperthermia, 1993;9:51-68. Int J Hyperthermia. 2009;25(7):512–516. doi: 10.3109/02656730903183445.

[8] Jordan A, Wust P, Fähling H, et al. Inductive heating of ferrimagnetic particles and magnetic fluids—physical evaluation of their potential for hyperthermia. Int J Hyperthermia. 1993;9(1):51–68. doi: 10.3109/02656739309061478.

[9] Dennis CL, Ivkov R. Physics of heat generation using magnetic nanoparticles for hyperthermia. Int J Hyperthermia. 2013;29(8): 715–729. doi: 10.3109/02656736.2013.836758.

[10] Soetaert F, Korangath P, Serantes D, et al. Cancer therapy with iron oxide nanoparticles: agents of thermal and immune therapies. Adv Drug Deliv Rev. 2020;163–164:65–83. doi: 10.1016/j.addr.2020.06.025.

[11] Thiesen B, Jordan A. Clinical applications of magnetic nanoparticles for hyperthermia. Int J Hyperthermia. 2008;24(6):467–474. doi: 10.1080/02656730802104757.

[12] Andreu I, Natividad E. Accuracy of available methods for quantifying the heat power generation of nanoparticles for magnetic hyperthermia. Int J Hyperthermia. 2013;29(8):739–751. doi: 10.3109/02656736.2013.826825.

[13] Wells J, Ortega D, Steinhoff U, et al. Challenges and recommendations for magnetic hyperthermia characterization measurements. Int J Hyperthermia. 2021;38(1):447–460. doi: 10.1080/02656736.2021.1892837.

[14] Brem RF. Radiofrequency ablation of breast cancer: a step forward. Radiology. 2018;289(2):325–326. doi: 10.1148/radiol.2018181784.

[15] van de Voort EM, Struik GM, Birnie E, et al. Thermal ablation as an alternative for surgical resection of small (≤2 cm) breast cancers: a meta-analysis. Clin Breast Cancer. 2021;21(6):e715–e730. doi: 10.1016/j.clbc.2021.03.004.

[16] Zulkifli D, Manan HA, Yahya N, et al. The applications of high-intensity focused ultrasound (HIFU) ablative therapy in the treatment of primary breast cancer: a systematic review. Diagnostics (Basel). 2023;13(15):2595. doi: 10.3390/diagnostics13152595.

[17] van de Voort EMF, Struik GM, Koppert LB, et al. Treatment of early-stage breast cancer with percutaneous thermal ablation, an open-label randomised phase 2 screening trial: rationale and

design of the THERMAC trial. BMJ Open. 2021;11(9):e052992. doi: 10.1136/bmjopen-2021-052992.

[18] García-Tejedor A, Guma A, Soler T, et al. Radiofrequency ablation followed by surgical excision versus lumpectomy for early stage breast cancer: a randomized phase II clinical trial. Radiology. 2018;289(2):317–324. doi: 10.1148/radiol.2018180235.

[19] Alphandéry E. Perspectives of breast cancer thermotherapies. J Cancer. 2014;5(6):472–479. doi: 10.7150/jca.8693.

[20] Hilger I, Andrä W, Hergt R, et al. Magnetische thermotherapie von tumoren der brust: ein experimenteller therapieansatz. Rofo. 2005;177(4):507–515. doi: 10.1055/s-2005-858021.

[21] Maier A, van Oossanen R, van Rhoon GC, et al. From structure to function: understanding synthetic conditions in relation to magnetic properties of hybrid Pd/Fe-oxide nanoparticles. Nanomaterials (Basel). 2022;12(20):3649. doi: 10.3390/nano12203649.

[22] van Oossanen RG, Brown JMC, Maier A, et al. Feasibility study on the radiation dose by radioactive magnetic core-shell nanoparticles for open-source brachytherapy. Cancers (Basel). 2022;14(22): 5497. doi: 10.3390/cancers14225497.

[23] Meattini I, Becherini C, Boersma L, et al. European society for radiotherapy and oncology advisory committee in radiation oncology practice consensus recommendations on patient selection and dose and fractionation for external beam radiotherapy in early breast cancer. Lancet Oncol. 2022;23(1):e21–e31. doi: 10.1016/S1470-2045(21)00539-8.

[24] Atkinson WJ, Brezovich IA, Chakraborty DP. Usable frequencies in hyperthermia with thermal seeds. IEEE Trans Biomed Eng. 1984; 31(1):70–75. doi: 10.1109/TBME.1984.325372.

[25] Dutz S, Hergt R. Magnetic nanoparticle heating and heat transfer on a microscale: basic principles, realities and physical limitations of hyperthermia for tumour therapy. Int J Hyperthermia. 2013; 29(8):790–800. doi: 10.3109/02656736.2013.822993.

[26] Natividad E, Castro M, Mediano A. Adiabatic vs. non-adiabatic determination of specific absorption rate of ferrofluids. J Magn Magn Mater. 2009;321(10):1497–1500. doi: 10.1016/j.jmmm.2009.02.072.

[27] Wildeboer R, Southern P, Pankhurst Q. On the reliable measurement of specific absorption rates and intrinsic loss parameters in magnetic hyperthermia materials. J Phys D: Appl Phys. 2014; 47(49):495003. doi: 10.1088/0022-3727/47/49/495003.

[28] Gonzalez-Fernandez M, Torres T, Andrés-Vergés M, et al. Magnetic nanoparticles for power absorption: optimizing size, shape and magnetic properties. J Solid State Chem. 2009;182(10): 2779–2784. doi: 10.1016/j.jssc.2009.07.047.

[29] Salunkhe AB, Khot VM, Pawar SH. Magnetic hyperthermia with magnetic nanoparticles: a status review. Curr Top Med Chem. 2014;14(5):572–594. doi: 10.2174/1568026614666140118203550.

[30] Deatsch AE, Evans BA. Heating efficiency in magnetic nanoparticle hyperthermia. J Magn Magn Mater. 2014;354:163–172. doi: 10.1016/j.jmmm.2013.11.006.

[31] Obaidat IM, Narayanaswamy V, Alaabed S, et al. Principles of magnetic hyperthermia: a focus on using multifunctional hybrid magnetic nanoparticles. Magnetochemistry. 2019;5(4):67. doi: 10.3390/magnetochemistry5040067.

[32] Vassallo M, Martella D, Barrera G, et al. Improvement of hyperthermia properties of iron oxide nanoparticles by surface coating. ACS Omega. 2023;8(2):2143–2154. doi: 10.1021/acsomega.2c06244.

[33] Jiang Q, Ren F, Wang C, et al. On the magnetic nanoparticle injection strategy for hyperthermia treatment. Int J Mech Sci. 2022;235:107707. doi: 10.1016/j.ijmecsci.2022.107707.

[34] Salloum M, Ma R, Zhu L. Enhancement in treatment planning for magnetic nanoparticle hyperthermia: optimization of the heat absorption pattern. Int J Hyperthermia. 2009;25(4):309–321. doi: 10.1080/02656730902803118.

[35] Di Barba P, Dughiero F, Sieni E. Synthesizing distributions of magnetic nanoparticles for clinical hyperthermia. IEEE Trans Magn. 2012;48(2):263–266. doi: 10.1109/TMAG.2011.2174340.

[36] Tang Y-D, Jin T, Flesch RC, et al. Simultaneous optimization of injection dose and location for magnetic hyperthermia using metaheuristic algorithms. IEEE Trans Magn. 2020;56(1):1–6. doi: 10.1109/TMAG.2019.2949933.

[37] Rodrigues HF, Capistrano G, Bakuzis AF. In vivo magnetic nanoparticle hyperthermia: a review on preclinical studies, low-field nano-heaters, noninvasive thermometry and computer simulations for treatment planning. Int J Hyperthermia. 2020;37(3):76–99. doi: 10.1080/02656736.2020.1800831.

[38] Hergt R, Dutz S. Magnetic particle hyperthermia—biophysical limitations of a visionary tumour therapy. J Magn Magn Mater. 2007; 311(1):187–192. doi: 10.1016/j.jmmm.2006.10.1156.

[39] Singh S, Melnik R. Thermal ablation of biological tissues in disease treatment: a review of computational models and future directions. Electromagn Biol Med. 2020;39(2):49–88. doi: 10.1080/15368378.2020.1741383.

[40] Soetaert F, Kandala SK, Bakuzis A, et al. Experimental estimation and analysis of variance of the measured loss power of magnetic nanoparticles. Sci Rep. 2017;7(1):6661. doi: 10.1038/s41598-017-07088-w.